Breccia dikes and crater-related faults in impact craters on Mars: Erosion and exposure on the floor of a crater 75 km in diameter at the dichotomy boundary

James W. HEAD[*] and John F. MUSTARD

Department of Geological Sciences, Brown University, Providence, Rhode Island 02912, USA
[*]Corresponding author. E-mail: James_Head@brown.edu

Abstract–Environmental conditions on Mars are conducive to the modification and erosion of impact craters, potentially revealing the nature of their substructure. On Earth, postimpact erosion of complex craters in a wide range of target rocks has revealed the nature and distribution of crater-related fault structures and a complex array of breccia and pseudotachylyte dikes, which range up to tens of meters in width and tens of kilometers in length. We review the characteristics of fault structures, breccia dikes, and pseudotachylyte dikes on Earth, showing that they occur in complex network-like patterns and are often offset along late-stage crater-related faults. Individual faults and dikes can undulate in width and can branch and bifurcate along strike. Detailed geological analyses of terrestrial craters show that faults and breccia dikes form during each of the major stages of the impact-cratering process (compression, excavation, and modification). We report here on the discovery of prominent, lattice-like ridge networks occurring on the floor of a highly modified impact crater 75 km in diameter near the dichotomy boundary of the northern lowland and southern upland. Interior fill and crater-floor units have been exhumed by fluvial and eolian processes to reveal a unit below the crater floor containing a distinctive set of linear ridges of broadly similar width and forming a lattice-like pattern. Ridge exposures range from ~1–4 km in length and ~65–120 m in width, are broadly parallel, straight to slightly curving, and are cross-cut by near-orthogonal ridges, forming a box or lattice-like pattern. Ridges are exposed on the exhumed crater floor, extending from the base of the wall toward the center. On the basis of the strong similarities of these features to terrestrial crater-related fault structures and breccia dikes, we interpret these ridges to be faults and breccia dikes formed below the floor of the crater during the excavation and modification stages of the impact event, and subsequently exhumed by erosion. The recognition of such features on Mars will help in documenting the nature of impact-cratering processes and aid in assessment of crustal structure. Faults and breccia dikes can also be used as data for the assessment of post-cratering depths and degrees of landform exhumation.

INTRODUCTION

Impact cratering is one of the most significant processes shaping planetary geomorphology, particularly in early planetary history (e.g., Grieve and Pesonen 1992; Melosh 1989). The keys to the nature of the impact-cratering process lie in the exposures on Earth of impact craters planed off to different depths by erosion (e.g., Dence et al. 1977), on the Moon in the exquisite preservation of pristine surface textures and fresh crater morphology formed without an atmosphere (e.g., Pike 1976; Howard 1974), and on Venus in the very well-preserved morphologies representing interaction of the ejecta and the atmosphere (e.g., Schultz 1992). On Mars, a wide range of distinctive lobate ejecta-deposit morphologies are interpreted to be related to substrate volatiles (e.g., Carr et al. 1977) or interaction of the ejecta with the atmosphere (e.g., Schultz and Gault 1979). However, active eolian processes (e.g., Greeley et al. 1992) and episodic fluvial activity on Mars (e.g., Baker et al. 1992), as well as regional blanketing and exhumation (e.g., Grant and Schultz 1990), have obscured the detailed fine-scale morphology of all but the most recent impact craters (e.g., McEwen et al. 2005). Thus, in using different planetary environments to study impact cratering, Mars tends to lie between the Earth and the Moon, with more gradation than the Moon, but much less planation than the Earth.

Recent Mars exploration has obtained high-resolution imaging, spectroscopy, and altimetry data that permit further analysis of impact-cratering deposits in much more detail than previously possible. These new data, combined with an increased understanding of the impact-cratering process and deposition/exhumation processes on Mars, has led to renewed interest in the role that Mars can play in further decoding important aspects of the cratering process. In this paper, we report on the discovery of a complex system of ridges on the floor of an impact crater that we interpret to be fault structures and breccia/pseudotachylyte dikes formed in concert with the impact-cratering event, and subsequently exhumed. We document the characteristics of these features, show the nature of the overlying deposits and their exhumation, develop criteria for distinguishing these features from magmatic dikes and other ridge-like features, and assess their role in the cratering process through comparison with terrestrial examples. As background, we first outline the nature of crater-related fault structures and breccia/pseudotachylyte dikes on Earth in order to develop criteria for their recognition on Mars.

CRATER-RELATED FAULT STRUCTURES IN TERRESTRIAL CRATERS

Analysis of terrestrial impact craters eroded to various levels reveals the presence of numerous impact-related fault networks delineating megablocks of the crater rim and floor. During the excavation and crater modification stages at pressures below the Hugoniot elastic limit, localized brittle faulting is the dominant style of deformation. Faults and fault zones have been mapped at many terrestrial impact craters (e.g., Fig. 1). At the heavily eroded Decaturville structure, an array of steeply dipping faults forms linear and intersecting box-like patterns in the crater interior (Fig. 6 in Offield and Pohn 1979). Similar structures are observed (Fig. 1) at Gosses Bluff (Fig. 3 in Milton et al. 1972), Sierra Madera (Fig. 20 in Wilshire et al. 1972), Upheaval Dome (Fig. 3 in Kriens et al. 1999; Fig. 9 in Kenkmann et al. 2005), and the Haughton impact structure (Fig. 2 in Osinski and Spray 2005). Collectively, these structures form linear features that are both radial and concentric to the crater, are of different lengths and levels of continuity, and can anastomose and bifurcate, sometimes with local en echelon orientations that permit reconstruction of the sense of shear.

Sometimes these features become zones of weakness due to brecciation and fragmentation along the fault zone. Often, however, the shear movement associated with the fault offset can produce rocks that are more competent than their host rocks and, hence, are likely to form morphological ridges upon erosion and exhumation. Mechanisms by which strength-hardening can occur in fault zones includes shear that causes brecciation and grain-size reduction and provides effective conduits for subsequent fluid transfer. Subsequent localized fluid transfer along fault-zone networks may lead to preferred sealing of these rocks, in particular in the presence of impact-induced thermal heating of fluids (see, for example, the Haughton impact structure; Osinski et al. 2005b). Tectonic faults (shear bands) mapped at several places on the Colorado Plateau provide examples of exposed faults that were preferentially hardened and today are expressed morphologically as ridges due to differential weathering (see Figs. 89–94 in Davis 1999).

BRECCIA/PSEUDOTACHYLYTE DIKE CHARACTERISTICS IN TERRESTRIAL CRATERS

Breccia dikes are a common feature in eroded terrestrial complex impact craters. In a classic study, Lambert (1981) proposed a classification system of breccia dikes in crystalline rocks distinguishing type A (ranging up to a few centimeters in width, consisting of small, rounded, commonly monomineralic fragments embedded in a cryptocrystalline matrix that often displays fluidal texture and that can be subdivided into liquid and solid particle flows) and type B (angular to subrounded rock, mineral and glass fragments with a wide size distribution in a matrix of similar but finer-grained material). Type A dikes are too small to be seen at current orbital resolutions but might be readily observed by landers and rovers. Type B dikes can be subdivided into monomict and polymict subtypes and the polymict dikes show both no wall displacement (B_1) and relative displacement of the fracture wall (B_2). B_2 dikes range from centimeters to meters wide and form simple, straight continuous dikes. B_1 dikes are very complex and variable in geometry and size. They bifurcate, anastomose, and show sharp changes in direction and thickness. On the basis of these characteristics and relationships, Lambert (1981) concluded that 1) breccia dikes are not limited to the central uplift zone, but influence large areas of the crater target area; 2) a single impact can produce several successive generations of fractures and breccia diking; 3) type A dikes form first as part of the initial shock compression; and 4) type B dikes form during and/or after pressure release in the modification phase, with B_1 dikes emplaced by high-energy intrusion into the transient crater as it grows, and B_2 dikes forming during the modification stage as blocks are displaced. Early-stage fracture-producing processes serve to reduce target strength and angle of internal friction, enhancing movement in the modification stage.

Impacted sedimentary rocks exhumed from even deeper levels show abundant evidence of breccia dike development, particularly in the central peak region. The Upheaval Dome structure in Utah, USA, exposes a complex sandstone dike network emplaced and injected during crater and central peak formation (Fig. 2) (Kenkmann 2003). The dike system is characterized by 1) extreme variations in thickness (0.1– 10 m) even over short distances, 2) decreasing mean dike
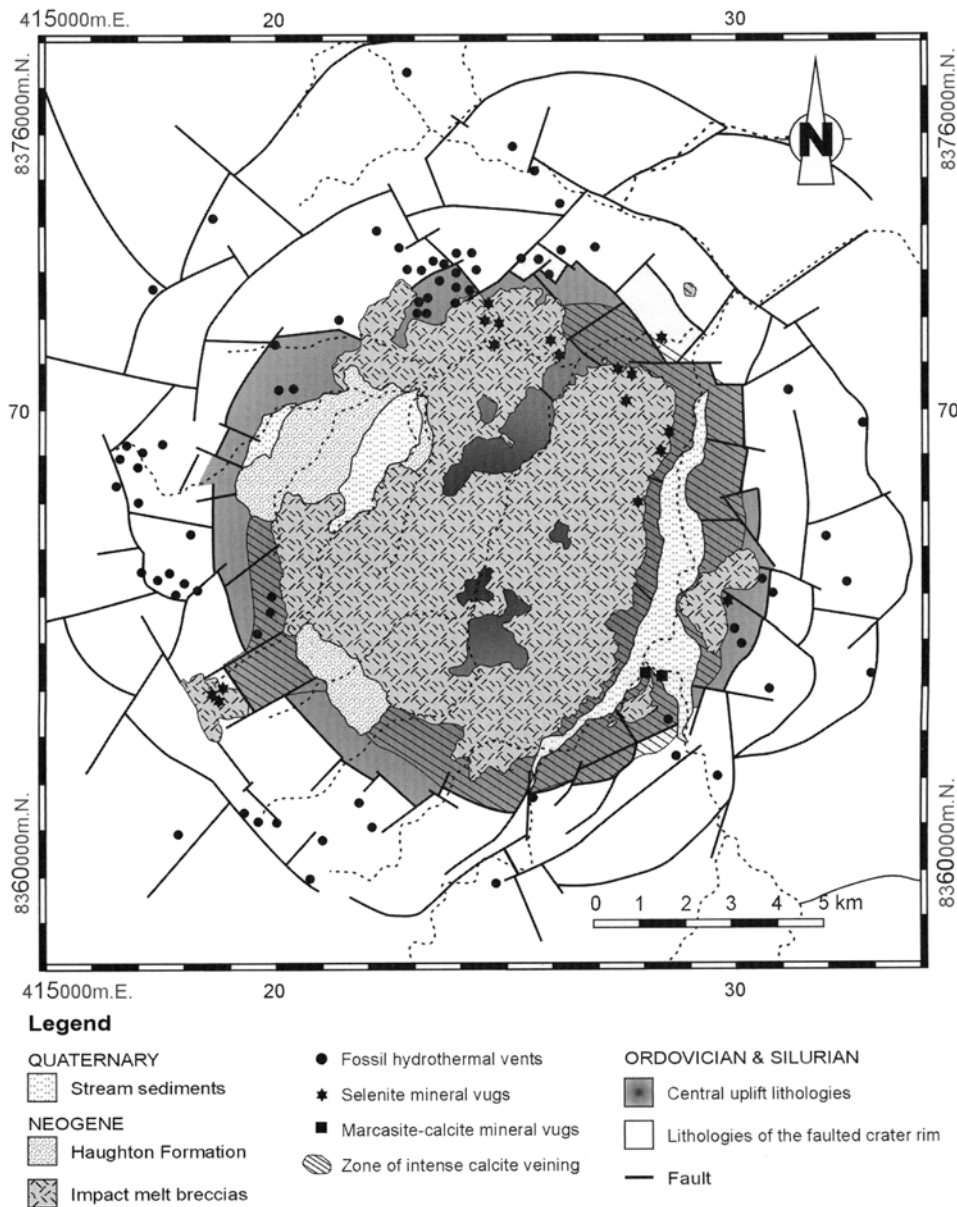
Fig. 1. A simplified geological map of the Haughton impact structure showing the major faults of the crater rim and their structural orientation in relation to overlying crater-floor impact-melt breccias, the regions of hydrothermal alterations and deposits, and subsequent stream erosion and sedimentary deposits. From Osinski et al. (2005b).

width with increasing distance from the crater center, 3) flow bulges with greatest thicknesses at nodular points, marking branch points where the dike bifurcates in two or more directions, 4) all forming a honeycomb-like, interconnected network of breccia dikes. Erosional outliers of dikes peripheral to the central peaks suggest that breccia dike networks were common throughout the crater subfloor at shallower levels.

Larger impact structures produce even wider and more extensive impact-related dikes. The Sudbury impact structure, which is 200–250 km in diameter, displays a series of steeply dipping dikes oriented radially and concentrically around the

structure. Known as the "Offset Dikes" because they often terminate and then reappear laterally offset by a few kilometers (Grant and Bite 1984), these features occupy footwall faults and fractures related to the excavation and modification stages of the impact event. One such dike feature, the Hess Offset, is at least 23 km long, 10–60 m wide, and located within and oriented subconcentrically to the large Sudbury crater. The dike is granodioritic, undulates in thickness along strike, and splays locally to form claw-shaped apophyses, originating during the modification stage of the impact event (Wood and Spray 1998). Similar Sudbury dikes are known, such as the Whistle-Parkin Offset Dike, which is
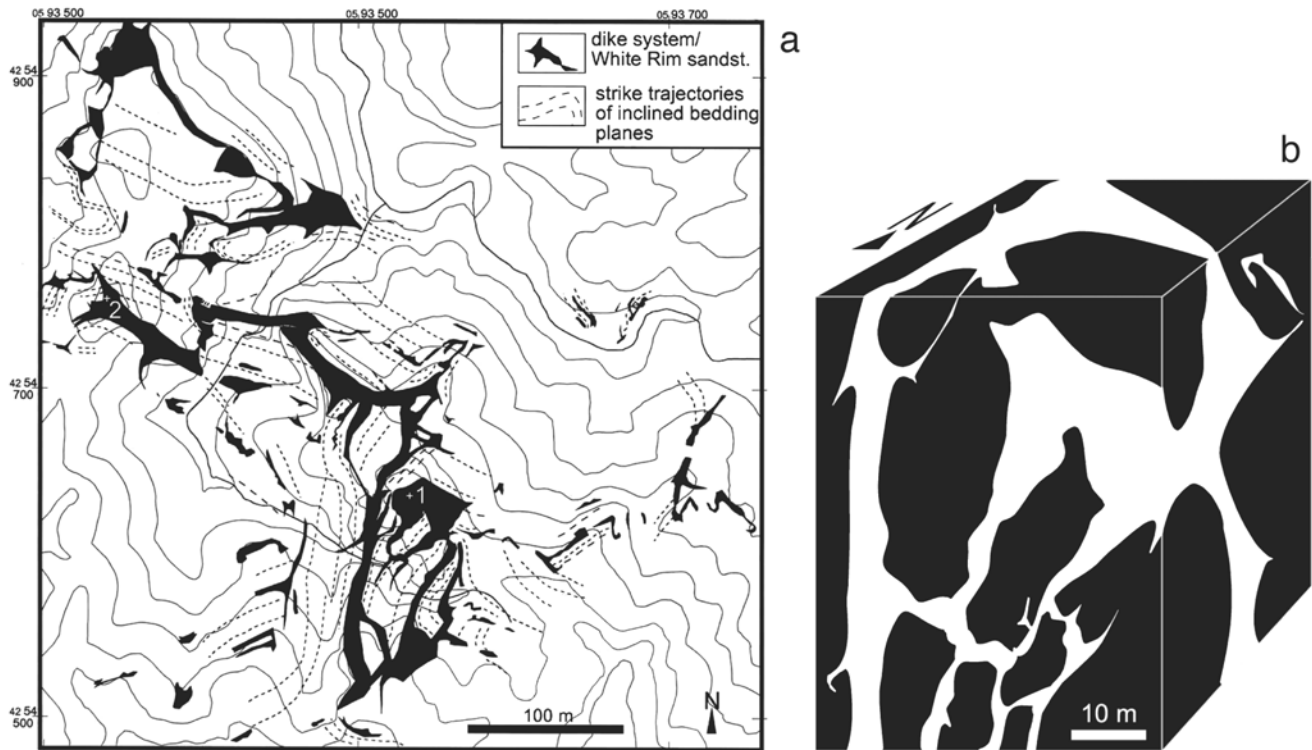
Fig. 2. a) The distribution of the White Rim sandstone dike system in the central uplift of the Upheaval Dome (from Kenkmann 2003). Note the linear, branching, and lattice-like networks associated with the dike systems. b) A sketch of a localized occurrence of the White Rim sandstone dike network (from Kenkmann 2003). Note the complex intersecting patterns and the linear, branching, and lattice-like networks.

12 km long and ~30 m wide (Murphy and Spray 2002), and the Foy Offset Dike, which is 36 km long, 50 m wide, and up to 400 m wide at the source (Tuchscherer and Spray 2002). Multistage emplacement (compression, excavation, and modification stages of the impact-cratering event) is implied for these dikes and the offsets are interpreted to be due to modification-stage crater adjustments.

Often encountered in larger impact structures are pseudotachylytes and breccia belts, which are in turn cut by breccia dikes. For example, at Sudbury, the South Range breccia belt is a breccia that is 45 km in length and tens to hundreds of meters in thickness with a very fine-grained matrix, interpreted to have been emplaced as a result of high strain-rate seismogenic slip during rim collapse of the Sudbury crater (Scott and Spray 2000; Spray and Thompson 1995; Thompson and Spray 1996), and often referred to as a "superfault" (Spray 1997).

In summary, breccia/pseudotachylyte dikes are seen in most of the eroded terrestrial complex craters and are developed in both crystalline and competent sedimentary target rocks (Lambert 1981). They are characterized by wide variations in petrology and mineralogy (commonly related to the target material and the stage in the cratering processes), and can range up to many tens of meters in thickness and tens of kilometers in length. They occur in complex lattice-like patterns and are often offset along late-stage crater-related

faults. Individual dikes can undulate in width and branch, anastomose and bifurcate along strike, and commonly show abruptly terminating injections. Although terrestrial weathering and vegetative cover inhibit complete mapping of breccia dikes, where detailed mapping has been done (e.g., Kenkmann 2003) breccia dikes can be comprehensively developed (Fig. 2) and drilling data on terrestrial craters further suggests that breccia dikes are very common (Lambert 1981).

GEOLOGICAL SETTING OF EXHUMED RIDGE NETWORKS ON MARS

The dichotomy boundary, separating the northern lowlands from the southern uplands, is an area of enhanced erosion and degradation of a variety of landforms, including impact craters (Tanaka et al. 2005). Over geological time, mass wasting, eolian, sapping, fluvial, tectonic, ground water, ground ice, and glacial processes have operated to modify the boundary (e.g., Sharp 1973; Squyres 1978; Lucchitta 1984; Carr 1995, 2001; McGill 2000; Mangold 2003; Head et al. 2005). We have examined a row of four aligned but nonoverlapping Noachian-aged impact craters, each 75–100 km in diameter, and extending along and adjacent to the dichotomy boundary over a distance of about 400 km (Fig. 3). Each impact crater shows a somewhat different state of

degradation, including heavily fractured floors, graben cutting the crater rims and floors, sapping channels and valleys eroding floors and rims and breaching craters, exhumed and stripped deposits on crater floors, completely breached crater rims, and extensive eolian deposition. Crater A (Fig. 3) has a floor dominated by multiple angular blocks; its rim has been breached by fluvial valleys both entering the crater (e.g., to the south) and exiting the crater (e.g., to the east). Crater B is the most heavily modified, with the northeast rim completely breached and open to the northern lowlands, and the floor deepened by erosion. Crater C has been modified by entering and departing channels and superposed impact craters, and Crater D has been modified by tectonic graben, sapping and fluvial channels. The different stages of modification are linked to the array of erosional processes operating along the dichotomy boundary since its formation in the early Noachian. Once craters on the upland plateau are breached by southward retreat of the dichotomy scarp, they become heavily modified and ultimately destroyed. We focus here on the modified floor of Crater C (Fig. 3), which is 75 km in diameter, and on an analysis of the complex arrays of ridge structures exhumed and exposed there.

GEOLOGICAL RELATIONSHIPS AND STRATIGRAPHY ON THE FLOOR OF CRATER C

Details of the morphology of the interior of Crater C are shown in Figs. 3 and 4. The crater interior is degraded with little evidence of the original crater interior morphology (sharp terraced walls and central peaks). The rim crest has been largely destroyed and the rim heavily modified by sapping valleys along the southwest and northwest margins (Fig. 4a). The northern rim, facing out into the northern lowlands, has been heavily modified on its exterior, eroded back and almost breached in several places. A network of valleys of apparent sapping origin modifies the southwestern rim and leads down the wall and onto the crater floor, producing a series of smooth, pond-like sedimentary deposits (Figs. 4e and 4f) superposed on crater-floor material. Located topographically lower, and apparently draining these deposits is a sinuous channel about 1–4 km in width (Fig. 4e) that winds its way across the floor, exiting the crater at a distinctive trough that completely breaches the northwest rim, leading onto the topographically lower floor of Crater B and out into the northern lowlands (Fig. 4a). A superposed impact crater is situated on the east-southeastern wall. Much of the floor of Crater C lies at an elevation of about −400 to −600 m. Slopes and the interior topography are typical of degraded craters (compare the Crater C wall slopes of less than 10° with those in excess of 10° in the superposed crater on the southeast wall; Fig. 4). The crater floor in the northeastern quadrant is higher (−100 to −400 m) than other parts of the floor and slopes toward the crater interior. The
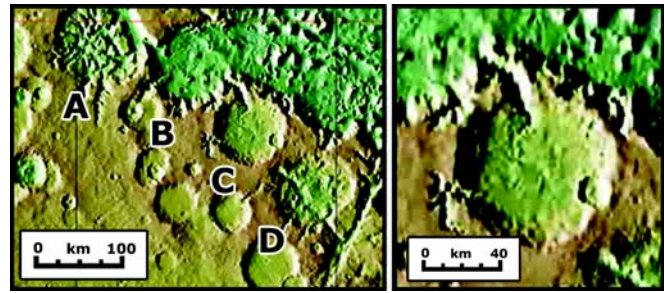

Fig. 3. Left: four impact craters (A–D, left to right) with different states of degradation at the dichotomy boundary. Right: Crater C, the subject of this analysis. MOLA gradient map.

southwestern quadrant of the floor is apparently embayed by a "delta-like" deposit at the mouth of the sapping channel network (see −400 m and −500 m contours in Figs. 4a and 4b). The remaining areas of the northwest and southern parts of the crater have been dissected and exhumed down to the levels of −350 to −650 m (Figs. 4 and 12). A sinuous channel cuts into these deposits down to depths of −650 to −970 m, and becomes progressively deeper as it exits the crater through the northwest rim. The floor slopes are generally less than 2°, except where the fluvial channel has cut the floor (Fig. 4c). The topographic map and profiles reveal the erosional characteristics described above and also show the terraced and mesa-like nature of the floor. THEMIS VIS and IR images reveal a large, ~12 km wide, relatively low-albedo (dark) patch of dunes and related eolian deposits in the northern part of the crater floor (Fig. 4e) at about −400 to −500 m elevation, and these images and MOC images reveal abundant local patches of relatively high-albedo (bright) dunes and patches on the crater floor and lining the floor of the sinuous channel (Figs. 6–8, 11). On the basis of the topography, slopes, and morphologic features, the degradational processes operating on this crater include mass wasting, sapping and fluvial processes, breaching and drainage, subsequent impact cratering, and eolian reworking.

The most highly degraded and dissected region of the crater floor is the western and northwest areas, where the networks of ridges occur (Fig. 4e). The details of this area revealed by high-resolution THEMIS and MOC images (Figs. 5–12) provide further insight into the stratigraphy of the units exposed there (Fig. 13), the evolution of the crater floor, and the history of the region. The youngest materials on the floor of the crater are of eolian origin and consist of the large low-albedo patch of dunes in the northern part of the floor (Fig. 4e), and abundant relatively high-albedo linear and arcuate dunes arranged in clusters and patches elsewhere on the crater floor (Figs. 6–8, 11). The very young age of these dune deposits is indicated by the apparent lack of superposed craters.

Underlying these eolian deposits is a regional, relatively smooth, flat-lying unit (the medial unit) that occurs over a significant portion of the crater floor (Fig. 13). Examination
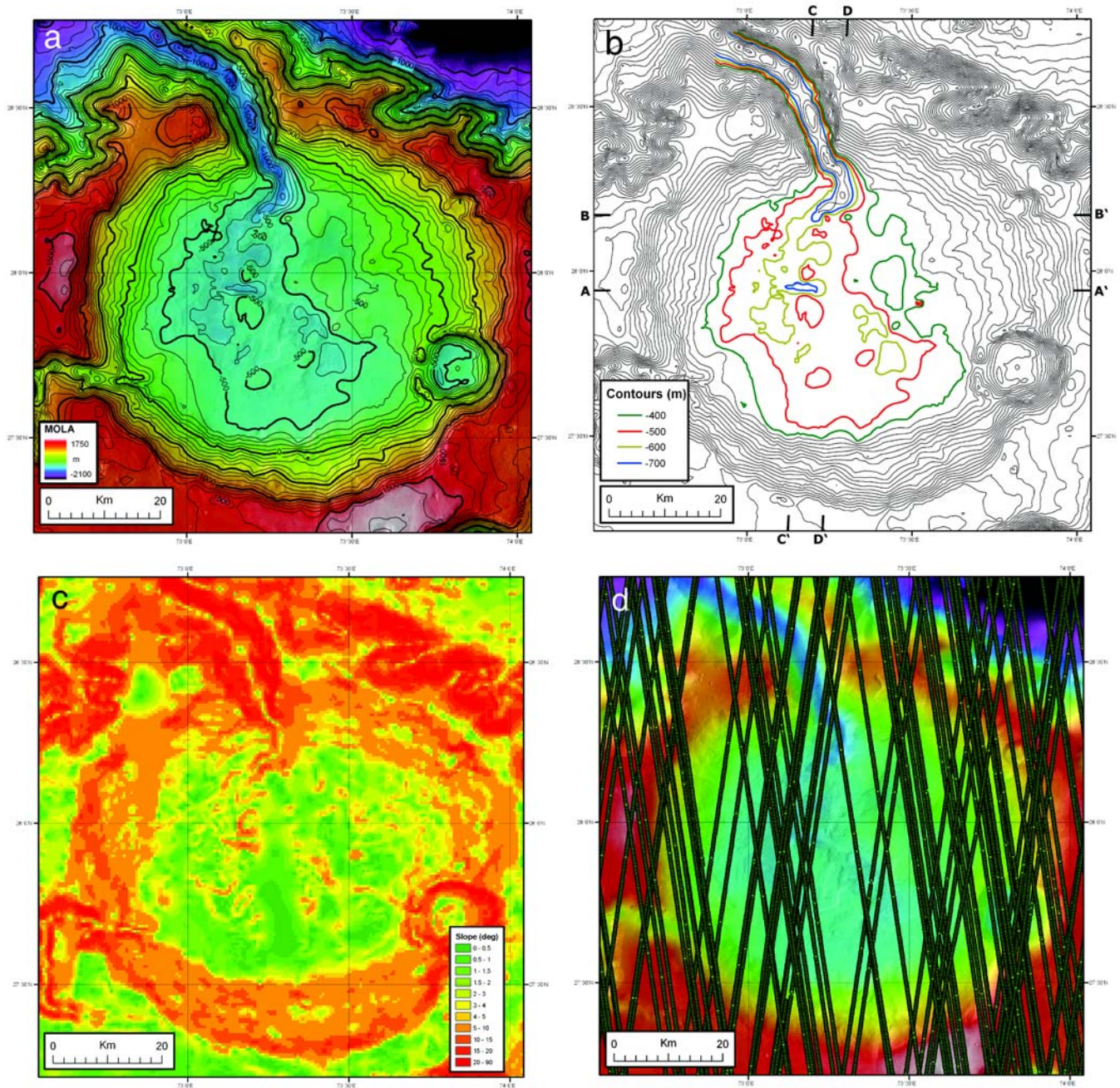
Fig. 4. Topographic, slope, and geologic maps of Crater C, with topographic profiles. a) A topographic map of Crater C from MOLA gridded altimetric data (1/128 pixels/degree), color-coded and contoured. Contour interval is 100 m, with bolder contour lines at 500 m intervals. b) Contour map only. Contour interval is 100 m. Key crater floor contours are color-coded. Compare to the profiles and dashed contour line locations in Fig. 4f. c) A slope map for Crater C and vicinity. Slopes derived from MOLA gridded topography (1/128 pixels/degree). d) The density of MOLA altimetric profiles in the Crater C region.

of the medial unit shows that it is composed of a flat-lying layered sequence that appears to have been partially stripped, exposing successively underlying layers within the unit (Fig. 5, lower right; Fig. 6, left; Fig. 9; Fig. 11, lower left and right; Fig. 12). In some places, this unit has been completely removed, exposing the lowermost unit, which consists of a distinctive network of lattice-like ridges (Figs. 5–11). The

thickness of the flat-lying medial unit determined from the altimetric profiles is of the order of 100–200 m and individual subunits within it range in thickness from a few meters to tens of meters. In the lower part of the medial unit there is a slightly hummocky, sometimes lineated, and moderately to highly cratered subunit. The lineated texture is composed of a series of parallel ridges and troughs similar to yardangs
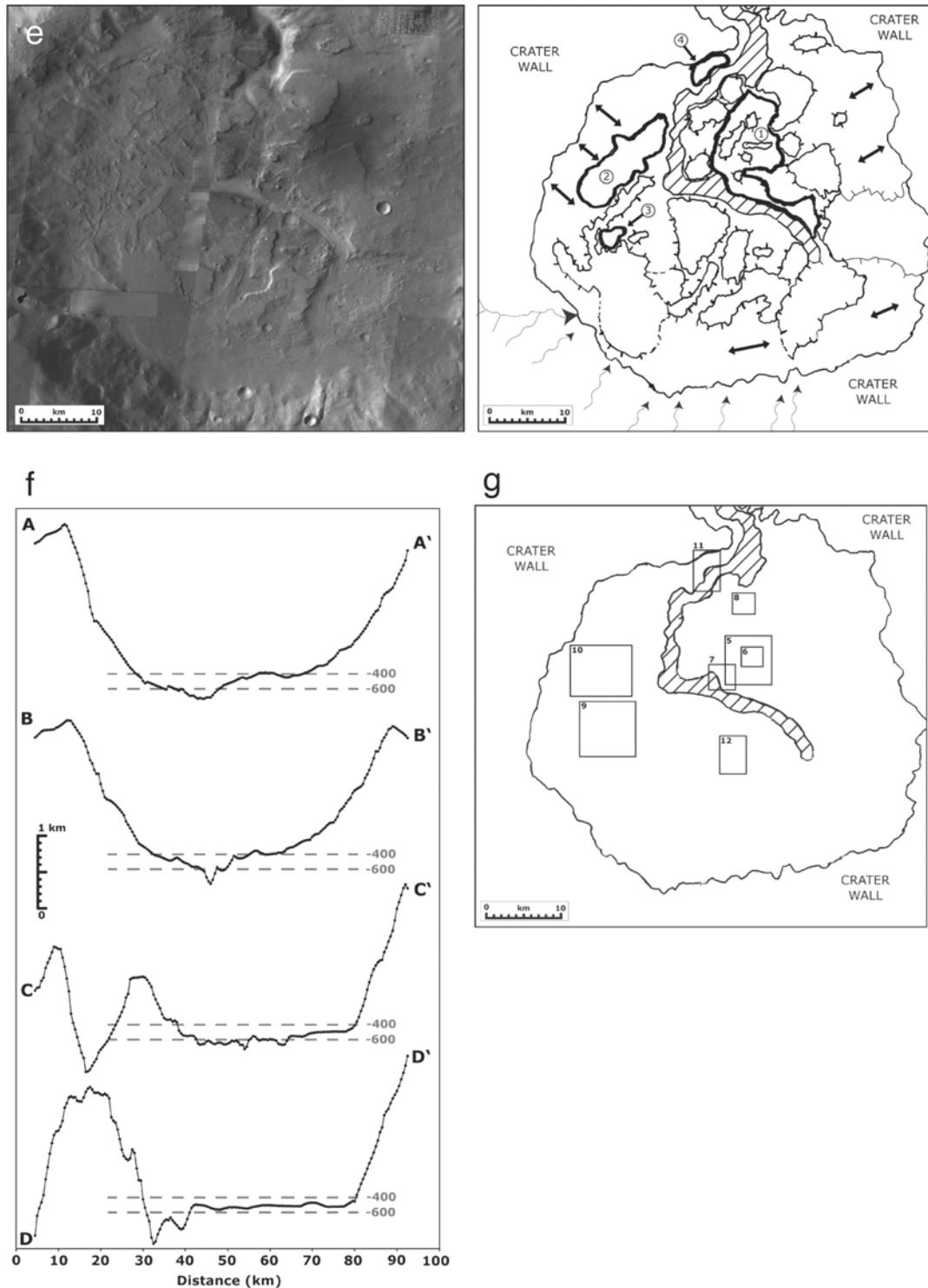
Fig. 4. *Continued*. Topographic, slope, and geologic maps of Crater C, with topographic profiles. e) A THEMIS mosaic and geological sketch map of the interior of Crater C. Thin lines with arrows indicate the location of sinuous channels in the southern crater wall. Bold arrows with double arrowheads show the general trend of yardang-like ridges and grooves. The numbered bold irregular outlined areas are regions of exposed linear, arcuate, and lattice-like ridges of the lowermost unit. Note that they generally occur in the lowest part of the crater, below the −450 m level. The obliquely ruled area is the floor of the sinuous channel draining the crater through the northwestern rim. Note the irregular depression 15 km in width at the head of the sinuous channel (southeast part of the crater floor). Irregularly shaped areas outlined with tick marks represent flat plateaus eroded down to various levels in the medial unit; tick marks point downslope. f) Altimetric profiles across the crater floor. See locations in Fig. 4b. g) Location map for MOC and THEMIS images and sketch maps shown in Figs. 5–12.
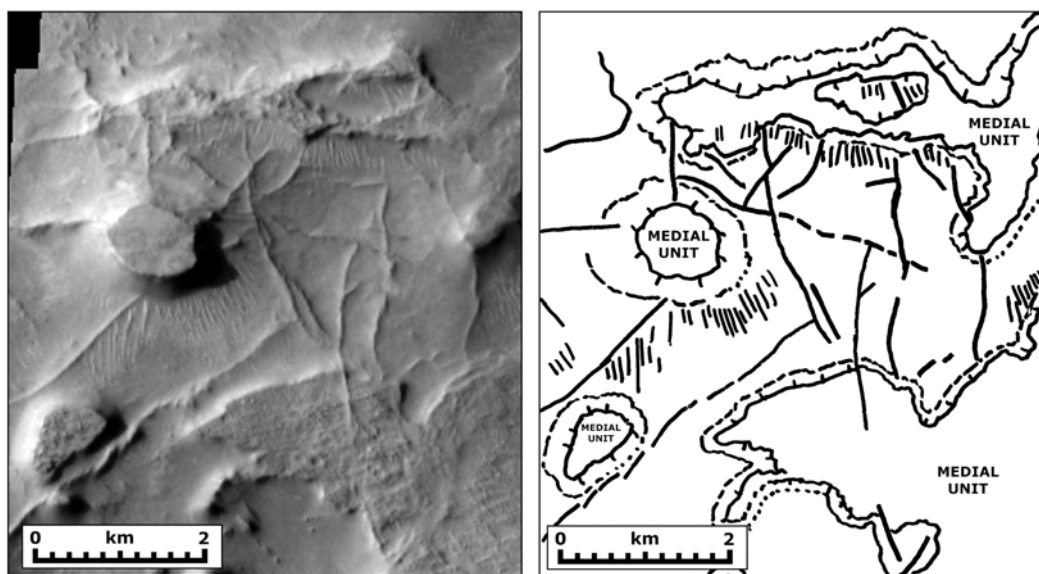
Fig. 5. An image of the floor of Crater C (area 1, Fig. 4e) and a sketch map showing plateaus and mesas of the medial unit, underlying ridge networks, and superposed dunes. Irregularly shaped hatchured lines are edges of plateaus and mesas, with hatchures on downslope side, and the dashed line marks the approximate base of the talus slope. Bold solid and dashed lines indicate differentially eroded ridges interpreted to be faults and breccia dikes. Short parallel lines mark the location of dunes. THEMIS image V12779010, 19 m/pxl. See Fig. 4g for location; crater center toward lower left.
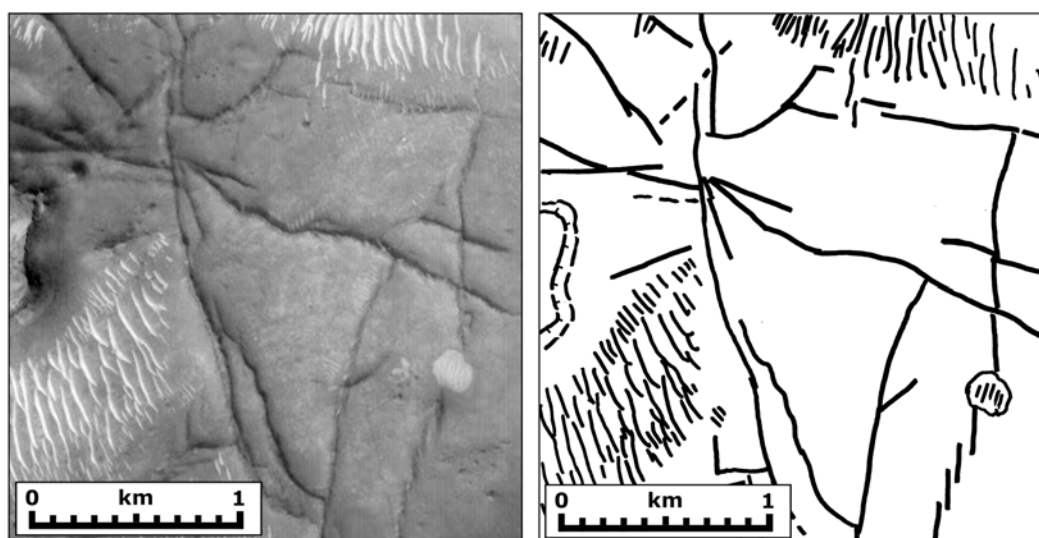

Fig. 6. An image of the floor of Crater C (area 1, Fig. 4e) showing a higher-resolution image and a sketch map of the area in the central part of Fig. 5 at the edge of the mesa in the left central part of the image (the irregularly hatchured line is the edge of the mesa, with hatchures on downslope side, and the dashed line marks the approximate base of talus slope). Short parallel lines mark the location of dunes. Bold solid and dashed lines indicate differentially eroded ridges that underlie the mesa and are interpreted to be faults and breccia dikes. Portion of MOC image E1401582, 6.4 m/pxl. See Fig. 4g for location; crater center toward lower left.

(Fig. 12, left). This surface appears to form a cap rock on some mesas of the medial unit, and thus appears to be competent in terms of its physical properties (Fig. 13). The high density of craters and competence suggest that this surface may have been the original surface of the crater floor, perhaps composed of the initial impact-melt breccia deposits. Some subunits form hummocky, relatively flat surfaces capping circular, elongate, and irregularly shaped mesas (Fig. 5, left, and Fig. 7, right) with relatively steep sides that are on the order of several tens to a hundred meters above the exhumed lattice-like unit. The lowermost medial subunit is rough surfaced (Fig. 5, lower right corner) and is transitional with the basal lattice-like unit with the ridges in the lattice appearing at the margins of the unit and becoming
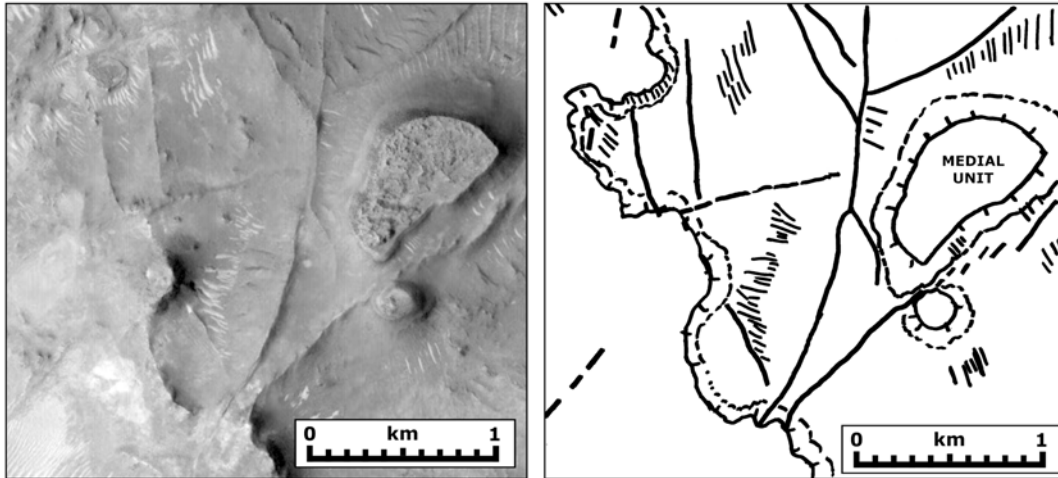
Fig. 7. The floor of Crater C (area 1, Fig. 4e) showing a higher-resolution image and a sketch map of the area in and adjacent to the southwest part of Fig. 5 in the vicinity of the mesa in the lower left part of the image (irregularly hatchured lines are the edges of the mesas and plateaus, with hatchures on downslope side, and the dashed line marks the approximate base of talus slope). Short parallel lines mark the location of dunes. Bold solid and dashed lines indicate differentially eroded ridges that underlie the mesas and plateaus and are interpreted to be faults and breccia dikes. A portion of MOC image R1800213, 6.4 m/pxl. See Fig. 4g for location; crater center toward bottom.
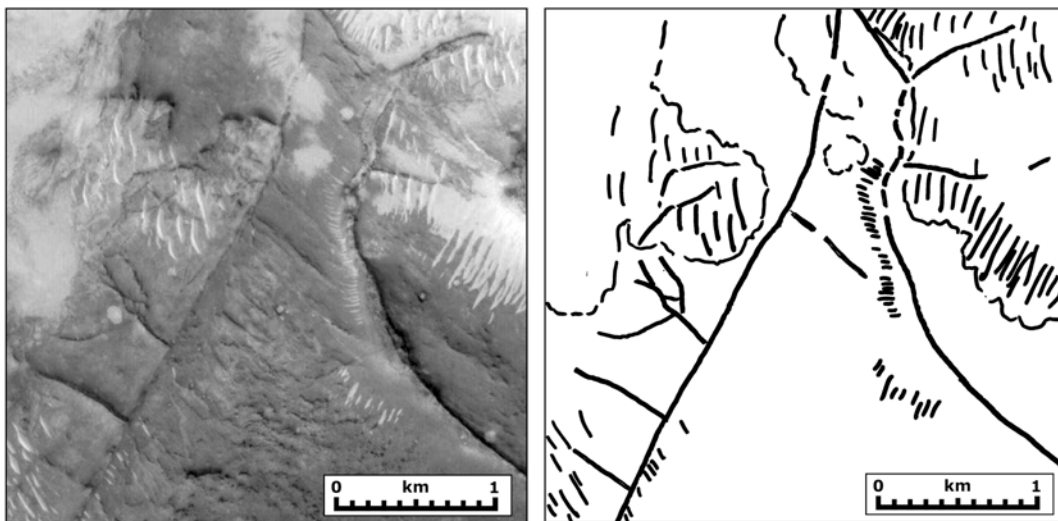

Fig. 8. The floor of Crater C (area 1, Fig. 4e) showing a high-resolution image and sketch map of the area north of Fig. 5 and largely below the topographic level of the mesas and plateaus of the medial unit. Short parallel lines mark the location of dunes, and enclosing lines represent areas where dune cover appears to be continuous. Bold solid and dashed lines indicate differentially eroded ridges that underlie the mesas and plateaus (not shown in this image) and interpreted to be faults and breccia dikes. A portion of MOC image E1401582, 6.4 m/pxl. See Fig. 4g for location; crater center toward bottom.

progressively exhumed with greater distance from the contact. This appears to represent the lowermost part of the coherent layer.

In summary, the medial unit weathers to large irregularly outlined areas with stepped and terraced margins (representing the subunits), and mesas that are rounded to oval in shape and up to ~1 km in diameter (Figs. 5–7). The nature of the medial unit suggests that it is flat-lying crater-floor fill, with the upper parts mostly derived from the fluvial deposits emplaced on the floor following crater formation by

sapping channels clearly seen on the southern and southwestern rim and wall (Fig. 4e, southern part of the image, and Figs. 5–12). These easily eroded units are the most likely source for the variety of dune deposits observed superposing them. The somewhat more competent (and more heavily cratered) layer seen at lower levels within this unit (Fig. 12, left) is interpreted to represent the more coherent impact-melt breccia deposits originally lining the cavity floor (Fig. 13). This setting of sedimentary deposits overlying impactites on the crater floor is very similar to the
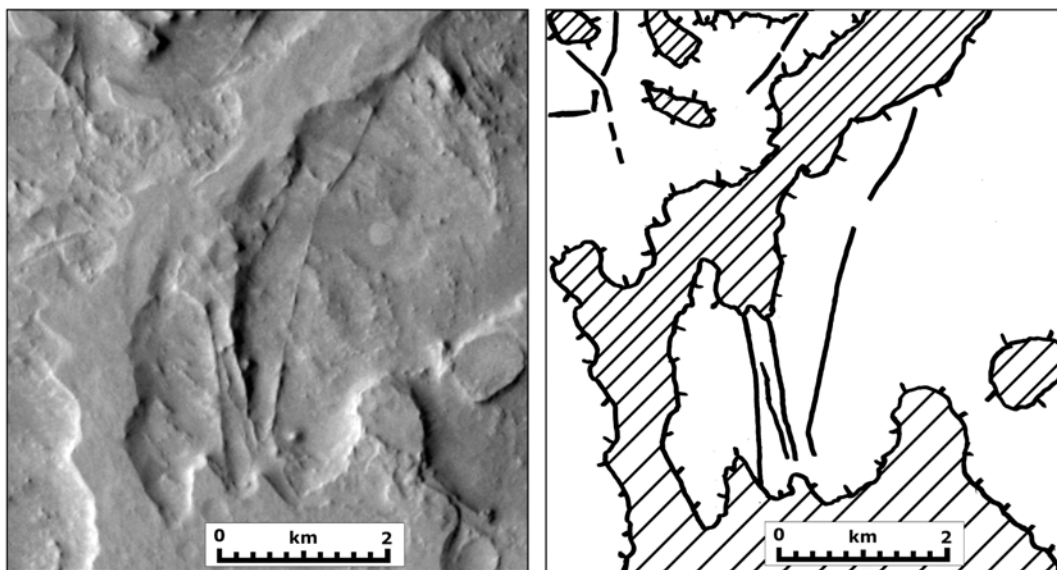
Fig. 9. An image of the floor of Crater C (area 3, Fig. 4e) and a sketch map showing linear ridges being exhumed from beneath a smooth-surfaced, steep-sided crater-floor deposit (obliquely ruled lines) representing the lower part of the medial unit. Irregularly hatchured lines are the edges of the mesas and plateaus of the medial unit, with hatchures on downslope side. Bold solid and dashed lines indicate differentially eroded ridges that underlie the plateau and mesa and are interpreted to be faults and breccia dikes. Portion of THEMIS image V10645015, 18 m/pxl. See Fig. 4g for location; crater center toward right.
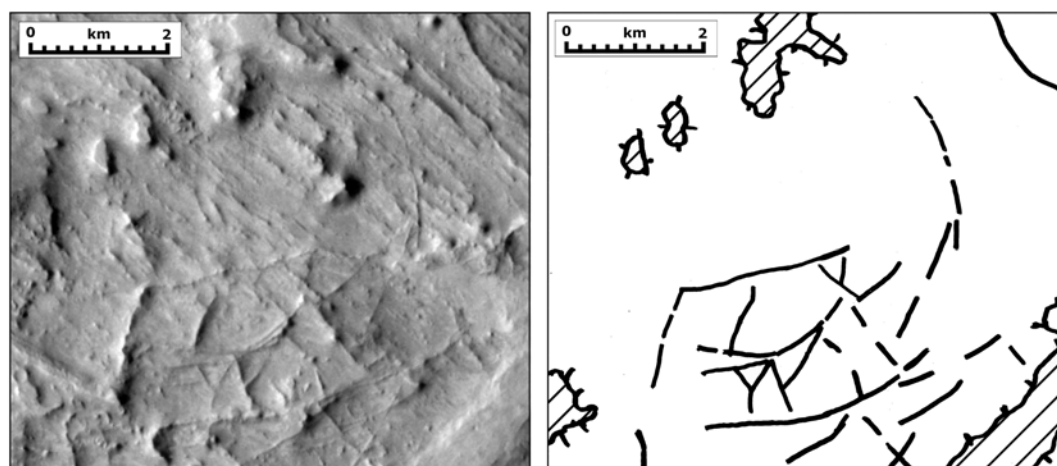

Fig. 10. An image of the floor of Crater C (area 2, Fig. 4e) and a sketch map showing linear ridges being exhumed from beneath smooth-surfaced, steep-sided mesas of crater-floor deposits (obliquely ruled lines). Irregularly hatchured lines are the edges of the mesas, with hatchures on downslope side. Bold solid and dashed lines indicate differentially eroded ridges that underlie the plateau and mesa and are interpreted to be faults and breccia dikes. More subtle, irregular, northwest-trending yardang-like ridges are interpreted to be due to wind erosion, which appears to be an important processe in stripping and exhumation. A portion of THEMIS image V10645015, 18 m/pxl. See Fig. 4g for location; crater center toward right.

stratigraphy reported in the Haughton impact structure in the Canadian High Arctic (e.g., Osinski et al. 2005a; Osinski and Lee 2005).

Underlying the medial unit, the lowermost unit contains a distinctive set of linear ridges of broadly similar width forming a lattice-like pattern (Fig. 4, areas labeled 1–4, and Figs. 5–11). In some areas (Fig. 5), the ridges form a chaotic lattice-like network with a wide range of parallel, branching and partly en echelon long and short ridges arrayed approximately concentric and radial to the crater (compare figure location to the crater center in Fig. 3g, and note the directions to the crater center in each figure caption). Details of this area (Fig. 6) show that the patterns increase in density and complexity with scale. Complex bifurcation of ridges and possible offsets are seen (Fig. 7, center), and in some areas abrupt terminations against other throughgoing ridges (Fig. 8)
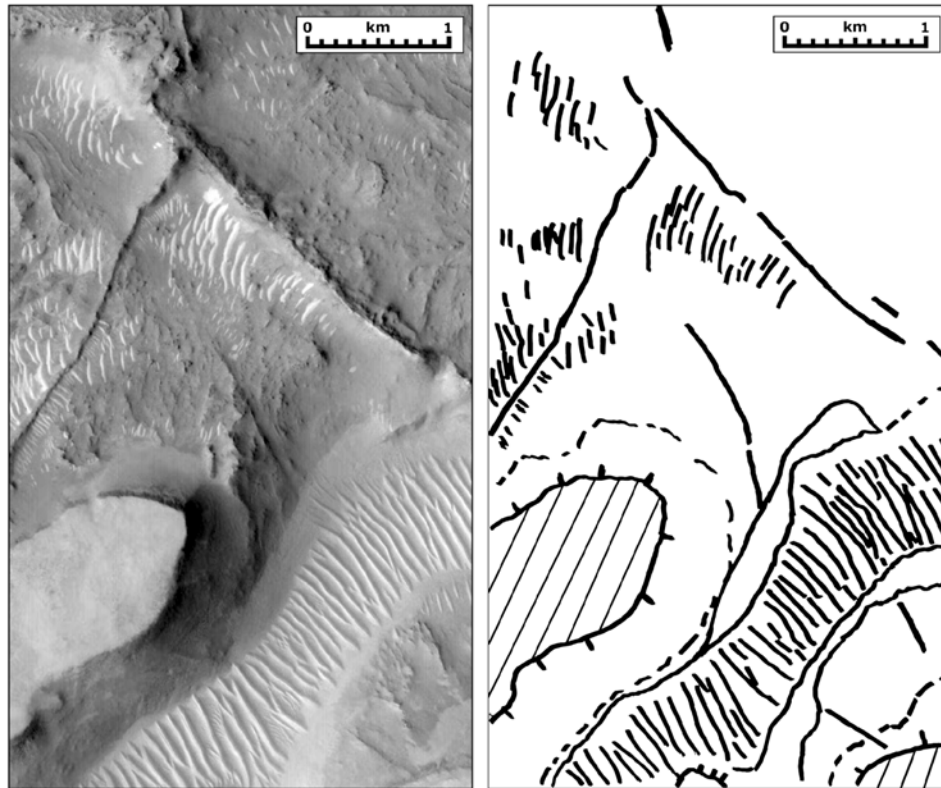
Fig. 11. An image of the floor of Crater C (area 4, Fig. 4e) and a sketch map showing linear ridges being exhumed from beneath smooth-surfaced, steep-sided mesas of crater-floor medial unit deposits (obliquely ruled lines). Irregularly hatchured lines are the edges of the mesa and plateaus of the medial unit, with hatchures are on the downslope side. The dashed line approximates the base of the slope. Short parallel lines mark the location of dunes. Note the strip of parallel dunes that occupy the floor of the sinuous channel (lower right). Bold solid and dashed lines indicate differentially eroded ridges that underlie the plateaus and mesas of the medial unit and are interpreted to be crater-related faults and breccia dikes. A portion of MOC image R1800213, 6.4 m/pxl. See Fig. 4g for location; crater center toward bottom.

suggest the presence of offsets. The contrast in morphology between the lowermost part of the medial unit and the lower ridged unit (Figs. 9 and 10) strongly suggests distinctly different characteristics. The presence of yardang-like features (Fig. 10) suggests that eolian processes are responsible for a significant part of the exhumation and exposure of the lattice-like ridges. Detailed views of the sinuous fluvial channel on the crater floor (Fig. 11) show that it cuts and postdates the formation of the medial unit and the lower lattice-like ridged unit (Fig. 13).

In summary, ridge exposures range from hundreds of meters to several kilometers in length and ~65–120 m in width; if the ridge represented a narrow vertical competent layer exposed by differential erosion, such as an igneous dike, this width would certainly overestimate the actual width due to the presence of a flanking erosional debris apron. Individual ridges are generally straight to slightly curving (Fig. 5–11), but some are slightly sinuous (Fig. 5, lower left, and Fig. 6, lower left). In some cases, they form broadly parallel ridges separated by hundreds of meters to a kilometer (Figs. 5, 6, and 9); in others, these ridges are cross-cut by near-orthogonal ridges forming a box or lattice-like pattern

(Figs. 5–8, 10). Some ridges terminate abruptly against other orthogonally oriented ridges (Figs. 8 and 10). Others bifurcate (Figs. 6 and 7), and a few show a possible en echelon structure (Fig. 5, lower left). Cross-cutting relationships are often clearly observed, but as yet no clear relationships have been established for sequential developments of trends. Near-orthogonal terminations suggest faulting and lateral offset, but exposure is insufficient to locate and restore possible offsets. The location of the exposed lattice-like unit is on the most heavily exhumed portions of the crater floor (approximately the NW quadrant) (Fig. 4e), extending from the base of the wall toward the center of the flat floor. The general orientation patterns are crudely radial and concentric to the crater.

On the basis of geological relations elsewhere on Mars, deposits characterizing crater interiors and fill might include initial impact-crater ejecta fallback, impact-melt and melt breccias lining the crater floor, subsequent distant ejecta, mass wasting, atmospheric dust and ice deposits, fluvial deposits, and volcanic tephra and lava flows. On the basis of the observed geological relationships (Figs. 4–12) and stratigraphy outlined here (Fig. 13), we interpret the
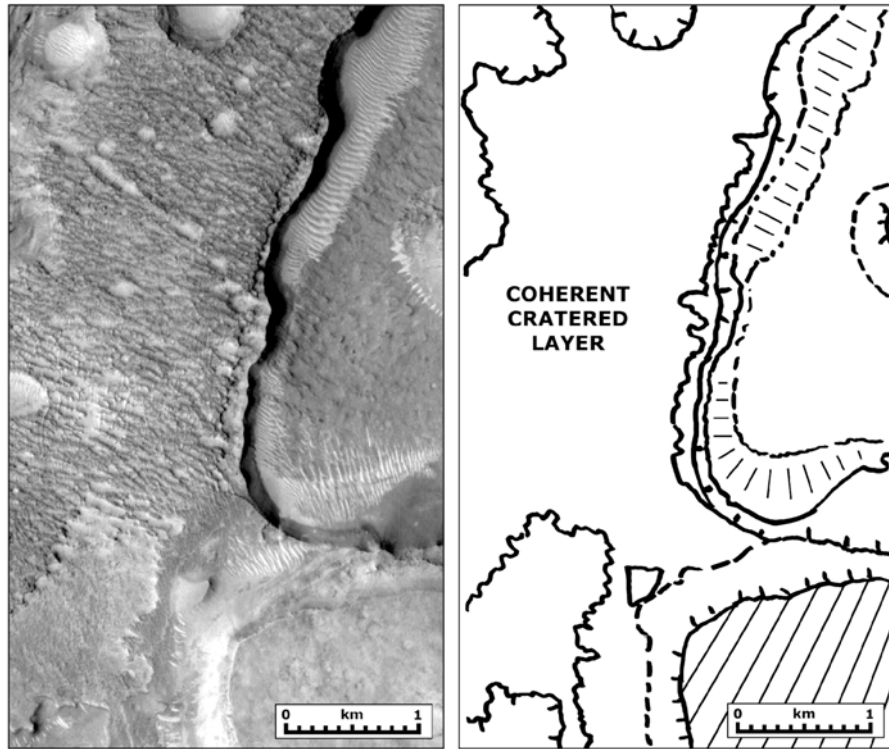
Fig. 12. An image of the floor of Crater C (area 1, Fig. 4e) and a sketch map showing a rough-surfaced, steep-sided, heavily cratered mesa of crater-floor deposits (left, middle, and upper). This deposit appears to be coherent (see scarps at margins) and to have been shaped by wind-sculpting (yardangs?). Located stratigraphically and topographically above this level (lower right of image) is another plateau surface in the medial unit (parallel-ruled surface); hatchured lines are the edges of the plateau, with hatchures are on the downslope side. The dashed line approximates the base of the slope. Short parallel lines are dunes. The coherent, cratered lower layer in the medial unit (left, middle, and upper) is interpreted to be more coherent impact melt of the initial crater floor, overlain by sedimentary crater fill (upper plateaus, lower right) and subsequently exhumed. A portion of MOC image R1800213, 6.4 m/pxl. See Fig. 4g for location.

lowermost unit in Crater C (the lattice-like unit) to represent the deepest portion of the fractured crater floor deposits, with erosion having cut into initial impact-melt breccia and later floor modification units to expose this material. The medial deposits are interpreted to represent a combination of units including lower friable impact-crater debris and breccias, a lower, more competent and heavily cratered unit thought to represent the lithified, impact-melt-rich floor deposits, and an upper, less-competent unit representing the sediments emplaced on the crater floor during formation of the channel deposits on the crater rim and partial crater floor filling (Fig. 13). Toward the end of the period of erosion and crater fill, the northwest crater rim was breached and the fluvial channel observed on the crater floor formed, draining the crater interior through the channel and eroding and removing crater floor material out of the crater and into the northern lowlands.

On the basis of the level of channel downcutting shown by the topographic relationships (Fig. 13; the channel cuts into the medial unit and to a level tens to hundreds of meters below the top of the lattice-like unit), the channel-forming fluvial events appear to have been a key factor in the modification of the northwest portion of the crater floor, in cutting through the competent cap rock within the medial unit and exposing the rest of the medial unit to erosion and eolian stripping. The distinctive bright dune deposits on the floor of the channel (Fig. 11) suggest that the channel-forming process removed and sorted significant volumes of floor material. Subsequent to channel formation, eolian processes have dominated erosion, with clear evidence of removal of material from the margins of scarps in the medial units, formation of yardang-like features, backwasting and formation of blowouts, and concentration of eroded material in bright and dark dunes and ergs.

ORIGIN OF RIDGES IN THE LOWERMOST LATTICE-LIKE UNIT

A number of origins have been suggested for the linear and arcuate ridges exposed on the surface of Mars. These origins can be subdivided into surface and subsurface types. Ridges interpreted to have formed at the surface include those resulting from contractional deformation creating arcuate and sinuous wrinkle ridges a few kilometers wide with smaller superposed sinuous ridges (e.g., Golombek et al. 1991; Watters 1991). The shape and form of such features,
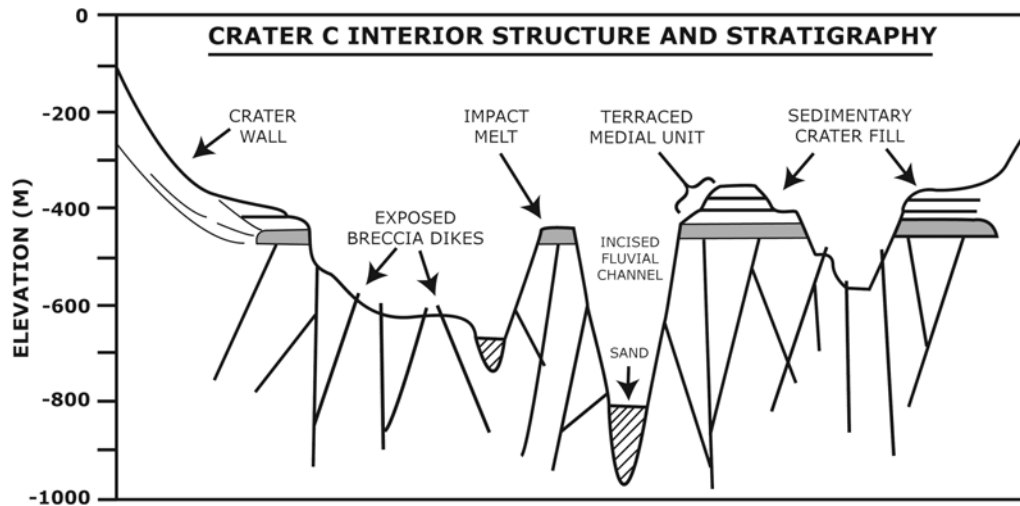
Fig. 13. A diagrammatic cross-section of Crater C interior and floor structure and stratigraphy, and interpretation of the origin of units and structures. During the initial excavation stage of the impact-crater-forming event, faults were formed and breccia dikes were injected into the crater floor; rebound and slumping in the modification stage created a second phase of fault formation and breccia dike emplacement as the crater assumed its final form and impact melt settled to the crater floor and solidified. Subsequently, fluvial erosion of the crater walls emplaced layers of sediments on the crater floor. When the northwest crater rim was breached by sapping and fluvial erosion, sediment was removed from the crater floor and the fluvial channel became deeply incised into the lower unit on the crater floor. Subsequently, eolian processes have continued to erode and expose the lower subfloor unit, preferentially exposing the contained crater-related faults and breccia dikes.

however, differs substantially from the ridges described here. Sinuous and arcuate ridges can also form as a result of sedimentary processes. Streams that produce channels with sediment that is coarser than surrounding deposits can sometimes be preferentially eroded to form ridges representing inverted stream deposits (e.g., Malin and Edgett 2003). Another possible sedimentary process is subglacial stream formation, resulting in eskers. Branching and dendritic sinuous ridges in the south circumpolar Dorsa Argentea Formation have been interpreted to be esker deposits (Head and Pratt 2001). However, the linear and lattice-like nature of the ridges described here argues against fluvial inverted stream and esker origins. More distinctly linear, ridge-forming features on Mars are observed around the margins of the lobate fans on the northwestern flanks of the Tharsis Montes (e.g., Zimbelman and Edgett 1992; Scott and Zimbelmann 1995; Head and Marchant 2003; Shean et al. 2005) and are interpreted as drop moraines of glacial origin. However, these features are formed of largely unconsolidated material, are susceptible to eolian erosion, and do not form the intersecting and lattice-like patterns described here.

Removal of overburden or younger deposits can exhume subsurface structures that then form ridges due to their more competent nature and differential weathering. The most commonly cited example is that of magmatic dikes intruded into country rock, which are then exposed by differential erosion of the substrate materials surrounding the dike. Some of the most well-known examples on Earth include the differentially eroded radial dike swarms of the Spanish Peaks, Colorado, USA (Smith 1987), and the parallel radial dikes of

the McKenzie dike swarms of Canada (Halls 1982; Fahrig and West 1986). Similar examples, interpreted to be the surface manifestation of exhumed dikes, have been documented on Mars in several different environments (e.g., Shean et al. 2005; Head et al. 2005, 2006; Basilevsky et al. 2005). A characteristic common to all of these examples of interpreted igneous dike exposure is that the ridges tend to form broad linear to broadly curved arching outcrops, rather than dense box-like and lattice-like networks. Dense box-like and lattice-like networks of igneous dikes could, however, form from repeated intrusion of magmatic dikes over extended periods of geological time due to changing stress fields. The position of these features just below the floor of a large impact crater, however, makes it highly unlikely that such a dense network would be preserved after the intense deformation and brecciation associated with impact crater interiors during crater formation. In fact, in recent studies the high level of disruption of signatures associated with pre-impact dikes has been used to help constrain the geometry and structures of poorly preserved craters in Australia and the Canadian Shield (e.g., l'Heureux et al. 2005).

Tectonic faults can also form distinctive linear zones (shear bands) that can become preferentially hardened and then be expressed morphologically as ridges due to differential weathering. Excellent examples of such distinctive ridge-like exposed faults have been mapped at several places on the Colorado Plateau (see Figs. 89–94 in Davis 1999). Although exhumation of regional throughgoing tectonic faults could take place, such features are unlikely to be preserved in such abundance on the floor of an impact crater.

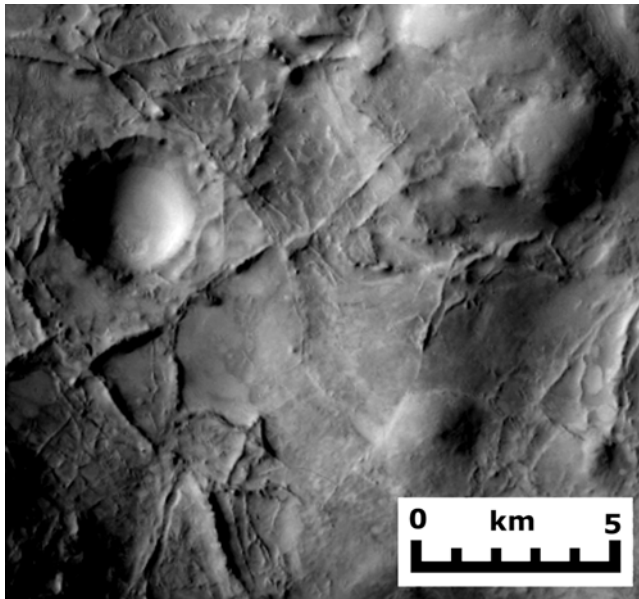On the basis of the distinctive characteristics of the

Fig. 14. A network of ridges interpreted to be crater-related faults and breccia dikes exposed on an exhumed portion of the floor of Crater D (see Fig. 3). A portion of THEMIS image V03555003, 37 m/pxl.

lattice-like unit described, its location in the interior of a large impact crater, and its exposure by exhumation of units just below the crater floor (Fig. 13), we prefer an interpretation related to the impact-cratering event itself. On Earth, as described above, two types of linear features are formed during the cratering event: 1) crater-related fault structures forming networks of linear, arcuate, and lattice-like faults (Offield and Pohn 1979; Milton et al. 1972; Wilshire et al. 1972; Kriens et al. 1999; Kenkmann et al. 2005; Osinski and Spray 2005), and 2) breccia dikes, common in eroded complex craters in a wide range of target rocks (Lambert 1981; Kenkmann 2003; Wood and Spray 1998). Breccia dikes range up to tens of meters in width and tens of kilometers in length, occur in complex lattice-like patterns, and are often offset along late-stage crater-related faults, and individual dikes can undulate in width and branch and bifurcate along strike. These characteristics are very similar to those of the ridges prominently occurring in the exhumed basal unit on the floor of the 75 km-diameter Crater C (Figs. 5–11, 13).

How did the specific arcuate ridges and lattice-like network on the floor of Crater C form? Analyses of terrestrial impact-crater deposits described above show that crater-related faults, breccia dikes, and pseudotachylyte dikes occur during both the formation and modification stages of the impact-cratering event. On the basis of the observed strong similarities between Crater C and terrestrial impact-crater faults and dikes, we interpret these ridges to be the manifestation of such features formed below the floor of the crater during the several stages of the impact event that created Crater C. Their nature and configuration suggest that they were largely formed during the excavation stage, when faults were formed and impact melts and breccias were injected into the subfloor in network-like dike patterns. Contemporaneously and immediately following this phase, the modification stage disrupted these earlier structures, offsetting them and forming new ones, often in complexly cross-cutting patterns. The ridges have been subsequently eroded and exhumed by the fluvial and eolian processes described above (Fig. 13). Hydrothermal processes (e.g., Osinski et al. 2005b) and subsequent cementation are candidates for making the features more resistant.

Are such networks expected to be common in other impact craters? Preliminary examination of the most highly eroded portions of adjacent crater floors reveals candidate examples of similar lattice-like network units in Crater D (e.g., Fig. 14). This suggests that similar impact craters that have undergone floor erosion and exhumation elsewhere on Mars may also reveal examples of faults and breccia/pseudotachylyte dikes, particularly with the newly available combination of high-resolution image data (THEMIS/MOC/HRSC).

The further study of the presence and characteristics of impact-crater-related faults and breccia dikes on Mars will help in documenting the nature of impact-cratering processes there and aid in assessment of the levels and depths of exhumation processes. For example, the location of the contact between exposed faults/breccia dikes and overlying more competent units provides a datum that is very likely to represent the stratigraphic position of the initial impact-crater floor. Thus, in heavily eroded and exhumed terrains, establishing this datum may provide a stratigraphic marker against which other processes of aggradation and degradation can be compared.

The presence of networks of faults and breccia dikes below complex crater floors also has important implications for the structure of the crust of Mars. For example, models of Mars crustal hydrology (e.g., Clifford 1993; Clifford and Parker 2001) need to take into account the development of significant lattice-like networks of solid dikes in considering the permeability of the impact-formed megaregolith and the potential global interconnectivity of the groundwater system.

On Earth, crater-related faults and breccia dikes are often associated with key mineral resources (e.g., Sudbury) and are also clearly related to late-stage thermal and mechanical readjustments of impact craters, thus forming candidate longer-term distributed heat sources analogous to magmatic hydrothermal vents (e.g., Osinski et al. 2005b). Upcoming very high spatial and spectral resolution instruments on MRO have the capability to analyze the geology and mineralogy of these types of breccia dikes in detail and document these potentially important sites of crustal alteration.

REFERENCES

Baker V. R., Carr M. H., Gulick V. C., Williams C. R., and Marley M. S. 1992. Channels and valley networks. In *Mars,* edited by Kieffer H. H., Jakosky B. M., Snyder C. W., and Matthews M. S. Tucson, Arizona: The University of Arizona Press. pp. 493–522.

Basilevsky A. T., Neukum G., Werner S., van Gasselt S., Gwinner K., and Ivanov B. A. 2005. Geology of the eastern flank of the Olympus Mons Volcano as seen in MEX HRSC images of Mars (abstract). 42nd Vernadsky/Brown Microsymposium on Comparative Planetology.

Carr M. H. 1995. The Martain drainage system and the origin of valley networks and fretted channels. *Journal of Geophysical Research* 100:7479–7507.

Carr M. H. 2001. Mars Global Surveyor observations of Martian fretted terrain. *Journal of Geophysical Research* 106:23,571–23,594.

Carr M. H., Crumpler L. S., Cutts J. A., Greeley R., Guest J. E., and Masursky H. 1977. Martian impact craters and emplacement of ejecta by surface flow. *Journal of Geophysical Research* 82: 4055–4065.

Clifford S. M. 1993. A model for the hydrologic and climatic behavior of water on Mars. *Journal of Geophysical Research* 98: 10,973–11,016.

Clifford S. M. and Parker T. J. 2001. The evolution of the Martian hydrosphere: Implications for the fate of a primordial ocean and the current state of the northern plains. *Icarus* 154:40–79.

Davis G. H. 1999. *Structural geology of the Colorado Plateau region of southern Utah, with special emphasis on deformation bands.* Boulder, Colorado: Geological Society of America. 157 p.

Dence M. R., Grieve R. A. F., and Robertson P. B. 1977. Terrestrial impact structures—Principal characteristics and energy considerations. Proceedings, 1st Symposium on Planetary Cratering Mechanics. pp. 247–275.

Fahrig W. F. and West T. D. 1986. Diabase dyke swarms of the Canadian Shield. Geological Survey of Canada Map #1627A. Scale 1:4,873,900.

Golombek M. P., Plescia J. B., and Franklin B. J. 1991. Faulting and folding in the formation of planetary wrinkle ridges. 21st Lunar and Planetary Science Conference. pp. 679–693.

Grant J. A. and Schultz P. H. 1990. Gradational epochs on Mars—Evidence from west-northwest of Isidis basin and Electris. *Icarus* 84:166–195.

Grant R. W. and Bite A. 1984. Sudbury quartz diorite offset dikes. In *The geology and ore deposits of the Sudbury structure,* edited by Pye E. G., Naldrett A. J., and Giblin P. E. Ontario, Canada: Ontario Geological Survey. pp. 275–300.

Greeley R., Lancaster N., Lee S., and Thomas P. 1992. Martian aeolian processes, sediments, and features. In *Mars,* edited by Kieffer H. H., Jakosky B. M., Snyder C. W., and Matthews M. S. Tucson, Arizona: The University of Arizona Press. pp. 730–766.

Grieve R. A. F. and Pesonen L. J. 1992. The terrestrial impact cratering records. *Tectonophysics* 216:1–30.

Halls H. C. 1982. The importance and potential of mafic dyke swarms in studies of geodynamic processes. *Geoscience Canada* 9:145–154.

Head J. W. and Pratt S. 2001. Extensive Hesperian-aged south polar ice sheet on Mars: Evidence for massive melting and retreat, and lateral flow and ponding of meltwater. *Journal of Geophysical Research* 106:12,275–12,300.

Head J. W. and Marchant D. R. 2003. Cold-based mountain glaciers on Mars: Western Arsia Mons. *Geology* 31:641–644.

Head J. W., Nahm A. L., Marchant D. R., Neukum G., and Team T. H. 2005. Modification of the dichotomy boundary on Mars by Amazonian mid-latitude regional glaciation. *Geophysical Research Letters,* doi:10.1029/2005GL024360.

Howard K. A. 1974. Fresh lunar impact craters—Review of variations with size. 5th Lunar Science Conference. pp. 61–69.

Kenkmann T. 2003. Dike formation, cataclastic flow, and rock fluidization during impact cratering: An example from the Upheaval Dome structure, Utah. *Earth and Planetary Science Letters* 214:43–58.

Kenkmann T., Jahn A., Scherler D., and Ivanov B. 2005. Structure and formation of a central uplift: A case study at the Upheaval Dome impact crater, Utah. In *Large meteorite impacts III,* edited by Kenkmann T., Horz F., and Deutsch A. Boulder, Colorado: Geological Society of America. pp. 85–115.

Kriens B., Shoemaker E. M., and Herkenhoff K. E. 1999. Geology of the Upheaval Dome impact structure, southeast Utah. *Journal of Geophysical Research* 104:18,867–18,887.

l'Heureux E., Ugalde H., Milkereit B., Boyce J., Morris W., Eyles N., and Artemieva N. 2005. Using vertical dikes as a new approach to constraining the size of buried craters: An example from Lake Wanapitei. In *Large meteorite impacts III,* edited by Kenkmann T., Horz F., and Deutsch A. Boulder, Colorado: Geological Society of America. pp. 43–50.

Lambert P. 1981. Breccia dikes—Geological constraints on the formation of complex craters. In *Multi-ring basins: Formation and evolution.* New York: Pergamon Press. pp. 59–78.

Lucchitta B. K. 1984. Ice and debris in the fretted terrain, Mars. *Journal of Geophysical Research* 89:409–419.

Malin M. C. and Edgett K. S. 2003. Evidence for persistent flow and aqueous sedimentation on early Mars. *Science* 302:1931–1934.

Mangold N. 2003. Geomorphic analysis of lobate debris aprons on Mars at Mars Orbiter Camera scale: Evidence for ice sublimation initiated by fractures. *Journal of Geophysical Research*, doi: 10.1029/2002JE001885.

McEwen A. S., Preblich B. S., Turtle E. P., Artemieva N. A., Golombek M. P., Hurst M., Kirk R. L., Burr D. M., and Christensen P. R. 2005. The rayed crater Zunil and interpretations of small impact craters on Mars. *Icarus* 176:351–381.

McGill G. E. 2000. Crustal history of north central Arabia Terra, Mars. *Journal of Geophysical Research* 105:6945–6960.

Melosh H. J. 1989. *Impact cratering: A geologic process.* New York: Oxford University Press. 253 p.

Milton D. J., Barlow B. C., Brett R., Brown A. R., Glickson A. Y., Manwaring E. A., Moss F. J., Sedmik C. E., van Son J., and Young G. A. 1972. Gosses Bluff impact structure, Australia. *Science* 175:1199–1207.

Murphy A. J. and Spray J. G. 2002. Geology, mineralization, and emplacement of the Whistle-Parkin Offset Dike, Sudbury. *Economic Geology* 97:1399–1418.

Offield T. W. and Pohn H. A. 1972. Geology of the Decaturville impact structure, Missouri. U. S. Geological Survey Professional Paper #1042. 48 p.

Osinski G. R. and Lee P. 2005. Intra-crater sedimentary deposits at the Haughton impact structure, Devon Island, Canadian High Arctic. *Meteoritics & Planetary Science* 40:1887–1900.

Osinski G. R. and Spray J. G. 2005. Tectonics of complex crater formation as revealed by the Haughton impact structure, Devon Island, Canadian High Arctic. *Meteoritics & Planetary Science* 40:1813–1834.

Osinski G. R., Spray J. G., and Lee P. 2005a. Impactites of the Haughton impact structure, Devon Island, Canadian High Arctic. *Meteoritics & Planetary Science* 40:1789–1812.

Osinski G. R., Lee P., Parnell J., Spray J. G., and Baron M. 2005b. A case study of impact-induced hydrothermal activity: The Haughton impact structure, Devon Island, Canadian High Arctic. *Meteoritics & Planetary Science* 40:1859–1878.

Pike R. J. 1976. Crater dimensions from Apollo data and supplemental sources. *Moon* 15:463–477.

Schultz P. H. 1992. Atmospheric effects on ejecta emplacement and crater formation on Venus from Magellan. *Journal of Geophysical Research* 97:16,183–16,248.

Schultz P. H. and Gault D. E. 1979. Atmospheric effects on Martian ejecta emplacement. *Journal of Geophysical Research* 84:7669–7687.

Scott D. H. and Zimbelman J. R. 1995. Geologic map of Arsia Mons volcano, Mars. U.S. Geological Survey Miscellaneous Investigation Series Map #I-2480. Scale 1:1,000,000.

Scott R. G. and Spray J. G. 2000 The south range breccia belt of the Sudbury impact structure: A possible terrace collapse feature. *Meteoritics & Planetary Science* 35:505–520.

Sharp R. P. 1973. Mars: Troughed terrain. *Journal of Geophysical Research* 78:4063–4083.

Shean D. E., Head J. W., and Marchant D. R. 2005. Origin and evolution of a cold-based tropical mountain glacier on Mars: The Pavonis Mons fan-shaped deposit. *Journal of Geophysical Research*, doi:10.1029/2004JE002360.

Smith R. P. 1987. Dyke emplacement at Spanish Peaks, Colorado. In *Mafic dyke swarms,* edited by Halls H. C. and Fahrig W. F. Geological Association of Canada Special Paper #34. pp. 47–54.

Spray J. G. 1997. Superfaults. *Geology* 25:579–582.

Spray J. G. and Thompson L. M. 1995. Friction melt distribution in a multiring impact basin. *Nature* 373:130–132.

Squyres S. W. 1978. Martian fretted terrain—Flow of erosional debris. *Icarus* 34:00–613.

Tanaka K. L., Skinner J. A., and Hare T. M. 2005. Geologic Map of the northern plains of Mars. U.S. Geological Survey Scientific Investations Map 2888. Scale 1:15,000,000.

Thompson L. M. and Spray J. G. 1996. Pseudotachylyte petrogenesis: Constraints from the Sudbury impact structure. *Contributions to Mineralogy and Petrology* 125:359–374.

Tuchscherer M. G. and Spray J. G. 2002. Geology, mineralization, and emplacement of the Foy Offset Dike, Sudbury impact structure. *Economic Geology* 97:1377–1397.

Watters T. R. 1991. Origin of periodically spaced wrinkle ridges on the Tharsis Plateau of Mars. *Journal of Geophysical Research* 96:15,599–15,616.

Wilshire H. G., Offield T. W., Howard K. A., and Cummings D. 1972. Geology of the Sierra Madera Cryptoexplosion Structure, Pecos County, Texas. U. S. Geological Survey Professional Paper #599-H. 42 p.

Wood C. R. and Spray J. G. 1998. Origin and emplacement of offset dykes in the Sudbury impact structure: Constraints from Hess. *Meteoritics & Planetary Science* 33:337–347.

Zimbelman J. R. and Edgett K. S. 1992. Volcanic and modified landforms on the Tharsis Montes, Mars (abstract #1581). 23rd Lunar and Planetary Science Conference. CD-ROM.